# Using Surface Pressure to Improve Tropical Cyclone Surface Wind Retrievals form Synthetic Aperture Radar Imagery

PI Ralph Foster
Applied Physics laboratory
University of Washington
1013 NE 40th St
Seattle, WA, 98105-6698
phone: (206) 685-5201     fax: (206) 543-6785     email: ralph@apl.washington.edu


Co-I Jerome Patoux
Department of Atmospheric Sciences
University of Washington
Box 351640
Seattle, WA, 9895-1640

**LONG-TERM GOALS**

The calibration and validation of surface wind and stress retrievals from oceanic synthetic aperture radar (SAR) imagery is especially difficult in tropical cyclone (TC) conditions. The geophysical model functions (GMFs) that characterize the radar backscatter in terms of the near-surface wind vector for different viewing geometries are currently poorly characterized for the very high wind and strong ocean surface wave conditions that are present in all TCs. Our long-term goal is to develop a novel methodology to use surface pressure observations and a planetary boundary (PBL) model for calibration and validation (Cal/Val) of SAR GMFs in TC conditions and to produce scene-wide wind vector retrievals that are most consistent with the image backscatter, the GMF and the PBL model. We further working toward an improved understanding of atmospheric boundary layer processes and air-sea interaction in tropical cyclones.

**OBJECTIVES**

The objectives of this research are to (1) develop the methodology for deriving TC SLP fields from first-guess surface wind vector estimates based on various GMF formulations; (2) Use these SLP fields to derive surface wind vector retrievals that are, in a least-squares sense, a scene-wide optimal surface wind retrieval that is consistent with the observable linear features in the SAR image, the GMF and the PBL model; (3) Develop an optimization scheme that seeks the minimum adjustment to the surface wind vector field that will minimize the difference between observed (e.g. via drop sondes or buoys) and SAR-derived bulk pressure gradients across the image. The optimized surface wind field can then be used either to assess or adjust the GMF.

| Report Documentation Page | | *Form Approved* *OMB No. 0704-0188* |
|---|---|---|

Public reporting burden for the collection of information is estimated to average 1 hour per response, including the time for reviewing instructions, searching existing data sources, gathering and maintaining the data needed, and completing and reviewing the collection of information. Send comments regarding this burden estimate or any other aspect of this collection of information, including suggestions for reducing this burden, to Washington Headquarters Services, Directorate for Information Operations and Reports, 1215 Jefferson Davis Highway, Suite 1204, Arlington VA 22202-4302. Respondents should be aware that notwithstanding any other provision of law, no person shall be subject to a penalty for failing to comply with a collection of information if it does not display a currently valid OMB control number.

| 1. REPORT DATE **30 SEP 2012** | 2. REPORT TYPE | 3. DATES COVERED **00-00-2012 to 00-00-2012** |
|---|---|---|

| 4. TITLE AND SUBTITLE **Using Surface Pressure to Improve Tropical Cyclone Surface Wind Retrievals form Synthetic Aperture Radar Imagery** | 5a. CONTRACT NUMBER |
|---|---|
| | 5b. GRANT NUMBER |
| | 5c. PROGRAM ELEMENT NUMBER |
| 6. AUTHOR(S) | 5d. PROJECT NUMBER |
| | 5e. TASK NUMBER |
| | 5f. WORK UNIT NUMBER |

| 7. PERFORMING ORGANIZATION NAME(S) AND ADDRESS(ES) **University of Washington,Applied Physics Laboratory,1013 NE 40th St,Seattle,WA,98105** | 8. PERFORMING ORGANIZATION REPORT NUMBER |
|---|---|

| 9. SPONSORING/MONITORING AGENCY NAME(S) AND ADDRESS(ES) | 10. SPONSOR/MONITOR'S ACRONYM(S) |
|---|---|
| | 11. SPONSOR/MONITOR'S REPORT NUMBER(S) |

| 12. DISTRIBUTION/AVAILABILITY STATEMENT **Approved for public release; distribution unlimited** |
|---|

| 13. SUPPLEMENTARY NOTES |
|---|

| 14. ABSTRACT |
|---|

| 15. SUBJECT TERMS |
|---|

| 16. SECURITY CLASSIFICATION OF: | | | 17. LIMITATION OF ABSTRACT | 18. NUMBER OF PAGES | 19a. NAME OF RESPONSIBLE PERSON |
|---|---|---|---|---|---|
| a. REPORT **unclassified** | b. ABSTRACT **unclassified** | c. THIS PAGE **unclassified** | **Same as Report (SAR)** | **16** | |

**Standard Form 298 (Rev. 8-98)**
Prescribed by ANSI Std Z39-18

**APPROACH**

GMFs describe the average radar backscatter from the sea surface in terms of the mean surface wind speed and the radar viewing geometry (incidence and azimuth angles). Compared to standard scatterometer wind vector retrievals, obtaining surface wind vectors from SAR imagery is very difficult. The same GMFs are used, but there is only a single viewing geometry for each wind vector cell. Wind directions are estimated by identifying linear features in the imagery at scales ranging from ~0.5 km to 2-4 km wavelengths. These linear features are assumed to be the surface imprint of PBL coherent structures that roughly align with the surface wind (Foster, 1997; 2005; Morrison et al., 2005; Lorsolo et al. 2008; Zhang et al. 2008; Ellis and Businger, 2010). These linear features cannot be identified throughout the entire SAR scene (which is commonly about 450 by 450 km), so wind directions are interpolated between the identified linear features using different methods. These directions and the backscatter are input to the GMF and wind speeds are retrieved. This product is the Raw wind retrieval.

Our research during the first year has performed in collaboration with Chris Wackerman of General Dynamics (GD) and Jochen Horstmann of NATO Undersea Research Centre (NURC). GD and NURC have developed separate methods for estimating wind directions. In addition, NURC has been developing "cross-pol" GMFs, which have a lot of promise in the high wind regime. The GD and NURC wind directions are merged into a single wind direction product and incorporated into a new processing system (WiSAR) that produces surface wind vector maps at 1 km spacing. We use the WiSAR wind vector fields as input to our SLP pattern and SLP-filtered surface wind retrieval system.

Because the pressure gradient force is a dominant term in the PBL momentum budget, the imprint of the surface stress field can be used to estimate the surface pressure gradient field through the use of a diagnostic PBL model. In its simplest form, PBL model assumes that the mean advective forces are relatively small and that the flow is neutrally-stratified and barotropic. The standard PBL model includes the effects of thermal winds, boundary layer stratification, a gradient wind correction for curved flow and momentum entrainment across the boundary layer top. We significantly improved the nonlinear dynamics representation in terms of a modified gradient wind correction for TC conditions, which added a second tuning parameter to the PBL model. We also developed and included an important correction for the inherent radial dependence of boundary layer depth in a strong swirling vortex consistent with the vortex boundary layer model developed in Foster (2009).

Once the pressure gradient fields have been obtained from the surface winds and the PBL model, a least-squares optimization technique is used to find the best-fit, zero-mean surface pressure pattern that matches the pressure gradient field. If pressure observations are available, the average difference between them and the zero-mean field is the least-squares optimal estimate of what is effectively the integration constant that results from converting pressure gradients into a pressure field.

The premise of using pressure data for SAR wind Cal/Val is based on the following fact: Even without using ancillary data to set the absolute value of the pressure field, the bulk pressure gradient (BPG) between any two points in the SAR-derived pressure field is the optimal estimate of that pressure difference derived from the input SAR winds. Because pressure is an integral property of the winds, pressure differences are more useful than point-by-point pressure comparisons assessing the quality of surface wind retrievals.

The derived SLP patterns may be used as inputs to the PBL model to re-derive an "SLP-filtered" surface wind field. This product is a scene-wide estimate of the surface wind vectors that enforces consistency between the all of the wind vectors and the pressure fields. We have extensively documented this overall methodology and the high quality of our SLP fields and derived wind vectors using QuikSCAT and ASCAT scatterometer wind vector data in several papers (Patoux et al. 2003; 2008; 2011).

Our applications to TC conditions with SAR wind vectors have shown that both the directions and speed in the SLP-filtered winds can be significantly changed when compared to the Raw wind input. In particular, the GMFs in TC conditions work best when the surface winds are across the radar beam and work poorly when the radar beam looks either up- or down-wind. The SLP-filtered winds "fill-in" the low wind holes near the TC core in these up- and down-wind regions. They can also fill in regions in the SAR WiSAR product that have been masked due to rainy conditions or for being out of range of the GMFs. Prior to the ITOP field campaign, we had only a handful of good SAR cases to study with near-in-time in situ data (dropsondes and stepped-frequency microwave radiometer, SFMR, surface wind speeds). Examination of these cases has shown that the SLP-filtered wind speeds are a major improvement over the input wind speeds. A qualitative inspection of the wind directions suggests that they are more realistic than the input directions, which tend to have too little inflow in the inner core region. However, validation of wind directions is severely limited by a lack of reliable data.

We pose the Cal/Val problem as an optimization problem in which we seek the minimum adjustment to the surface vector field that will minimize the difference between the SAR BPG and that derived from observations. A first-guess surface wind vector field from SAR is produced by WiSAR from which we calculate a first-guess surface pressure field. Given $N$ surface pressure observations within this field, e.g. from dropsondes or aircraft-deployed buoys, we can calculate multiple, $M = N(N-1)/2$, BPGs within the image. The cost function to be minimized is the RMS difference between the SAR-derived BPGs and the observations along with constraints on the corrections to the wind field so that the optimization procedure does not impose unreasonable wind vector corrections. Assuming $M$ BPG observations and $K$ total surface wind vectors, the cost function is:

$$J = \sum_{n=1}^{M} \left( \Delta P_n^S - \Delta P_n^O \right)^2 + w_1 \sum_{n=1}^{L} \left( S_n^{SAR} - S_n^{SFMR} \right)^2 + w_2 \sum_{n=1}^{K} \left| \mathbf{u}_n - \mathbf{u}_n^0 \right|^2 + \quad (1)$$

The first term represents the RMS difference between the SAR and observed BPGs. The second term minimizes the difference between the SAR and SFMR surface wind speeds. The third term measures the RMS vector magnitude of the corrections to the original surface wind field and acts as a smoothness constraint – it penalizes large, localized wind vector modifications.

Each optimization step adjusts the surface wind vectors and recalculates the surface pressure field and the BPGs. The optimization treats the $U$ and $V$ components of the SAR winds separately since their error characteristics are approximately independent and Gaussian (Freilich, 1997). The computation cost is nontrivial because each step in the optimization requires a new nonlinear surface pressure field in order to evaluate the cost function.

It should be emphasized that since surface pressure fields are integral properties of the surface vector wind fields, wind adjustments must occur over a broad spatial region rather than just locally near the pressure data. Thus, even though we use point wise pressure data, they imply wind corrections at a large number of wind vector cells.

**WORK COMPLETED**

The standard implementation of the hurricane SLP retrieval code and the SLP-filtered winds is in FORTRAN. However, we require an implementation version in Matlab in order to make use of its extensive optimization toolkit for research into the Cal/Val methodology. This has been completed by Patoux during Year 1. Foster has been working extensively on analyzing the in situ data (drop sondes and SFMR winds from C-130 flights) for use in evaluating the wind and pressure products and for developing the Cal/Val methodology. Foster developed a new method for estimating the mean surface wind from drop sondes. In the simplest cases it is consistent with the methods used for developing the SFMR model function (Uhlhorn et al., 2007). However, the ITOP experiment has provided a unique data set in which significant deviations from the assumptions in Uhlhorn et al. (2007) and the new methodology attempts to address these issues. The SAR data will provide a means of assessing how well the new technique works. A by-product of this analysis is estimates of the surface sensible and latent heat fluxes. We have been in contact with Prof. Shuyi Chen who is working on the heat flux estimates from ITOP.

An important aspect of the SLP-filtered wind fields is that they are smooth enough that reasonable derivative fields may be calculated. A striking feature in all of the SAR images that we have processed is ubiquitous, approximately flow-parallel alternating bands of surface wind convergence and divergence throughout the image. This pattern is broadly consistent with what would expected in a roll vortices-dominated PBL flow, which is the basic state of the tropical cyclone boundary layer (Foster, 2005). However, the implied wavelength in these convergence bands is roughly five times larger than would be expected from boundary layer rolls. We implemented a surface kinematic wind stress curl calculation and 10 km wavelength bandedness at these large aspect ratios (wavelength/boundary layer depth) is even more clearly evident. Foster developed a nonlinear wave-wave interaction theory for hurricane boundary layers, which is based on a simpler 2-D model developed by Mourad (1990), to explain how such large aspect ratio rolls could form.

**RESULTS**

*SLP-Filtered Winds*

An example of the SLP-filtered winds is shown in Figure 1. The raw SAR winds are shown in the left panel, the derived sea-level pressure pattern is shown in the right panel and the SLP-filtered winds are shown in the center panel. Note that the SLP-filtered winds modify both speed and direction compared to the raw winds. Superposed in shaded squares are wind speeds interpolated from the drop sonde profiles and the directions are shown as black vectors.
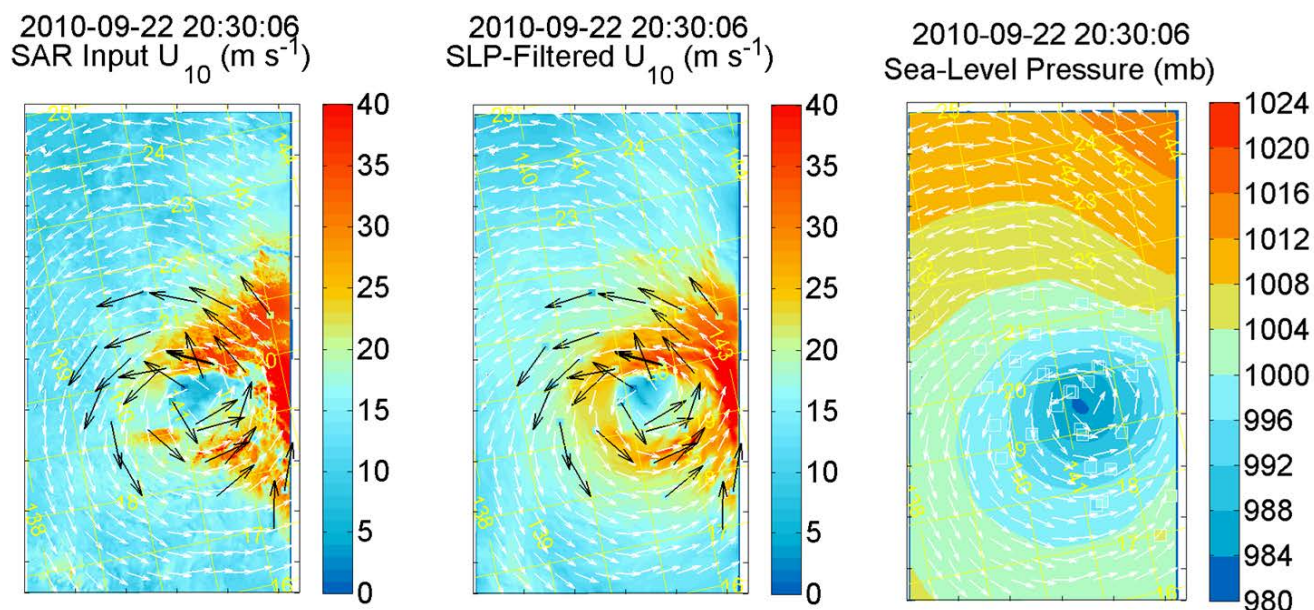
**Figure 1: SAR image of Typhoon Malakas, 22 Sep, 2010, 20:30. Left, raw SAR winds, Center: SLP-filtered winds; Right: derived SLP field. The winds are calculated for 1 km pixels. The white arrows are all the same length and show the SAR wind directions every 30 km. The black arrows are the track-corrected surface wind directions from the drop sondes. The track-corrected drop sonde surface pressures are shaded boxes in the right panel.**

The corresponding drop sonde bulk surface pressure differences compared to those calculated from the SAR winds are shown in the right panel of Figure 2. The scatter plot shows good correlation between the observed and derived bulk pressure gradients, which is the best test of the SLP pattern calculations and is the basis for using surface pressure as the basic tool for Cal/Val of SAR surface wind fields. Further improvement of the boundary layer model embedded within the SLP retrieval model may reduce the scatter in the BPG plot.
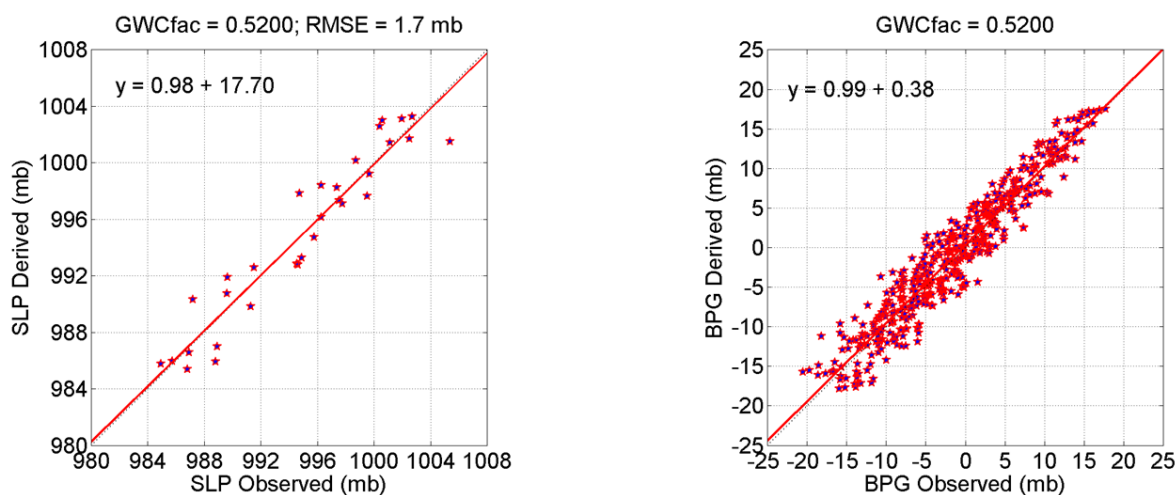


**Figure 2: Left: Scatterplot of observed and SAR-derived surface pressures; Right: scatterplot of observed and SAR-derived bulk pressure gradients (BPG).**

Figure 3 compares the SFMR surface wind speeds (black line) to the SAR derived winds. The SLP-filtered wind speeds (red line) agree better with the SFMR within the low incidence angle region NE of the storm center, than the raw winds (blue line) where the GMF had largely failed. The right panel shows the C130 calculation of the surface pressure. The SAR-derived SLP tracks these data well.

## 10-km Scale Hurricane Roll Vortices

Figure 4 shows surface wind convergence and the kinematic wind stress curl calculated from the SLP-filtered wind field of Super-Typhoon Megi just before landfall on Luzon. The scene is approximately 900 km long and 450 km wide. The $O(10 \text{ km})$ wavelength organization is evident in both products, but is clearest in the wind stress curl. Patterns like this are consistent with what would be expected from the approximately flow-parallel overturning circulations induced by boundary layer roll vortices. The scientific problem is that the organized convergence or wind stress curl fields imply a 10-km wavelength overturning circulation in the boundary layer, which is far outside known scale of tropical cyclone roll vortices.
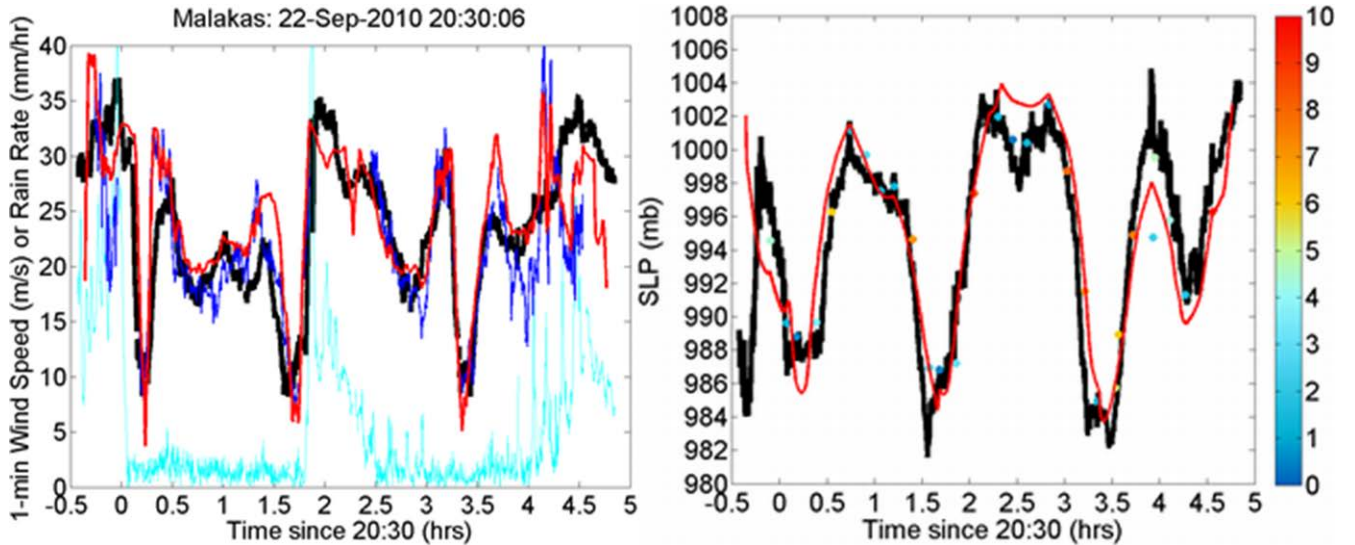


*Figure 3: Left: black, SFMR surface winds speeds; red: SLP-filtered wind speeds; blue: Raw wind speeds. The rain rate is the cyan line. Right: black: C130 surface pressure calculation; red: SAR-derived SLP.*

Theory (Foster, 2005) and observations (Morrison et al., 2005) shows that tropical cyclone boundary layers are ideal habitats for the growth and maintenance of $O(1 \text{ to } 3 \text{ km})$ wavelength roll vortices. The high shear and strong surface buoyancy flux is conducive to roll formation. Structures at ~2.4 aspect ratio grow much faster than rolls at longer or shorter wavelengths. However, Foster (2005) showed that a wide range of growing instabilities with wavelengths ranging from sub-km to $O(10 \text{ km})$ are capable of forming finite amplitude rolls. In this single-wave theory, wavelengths significantly larger or smaller than the dominant wavelengths would not survive the competition since the $O(1-3 \text{ km})$ wavelength rolls will reach the nonlinear growth stage and dominate the modified mean flow before the longer or shorter wavelength modes exhibit significant nonlinear growth. In order to compete, the longer wavelength modes must get an injection of energy to kick start them into the nonlinear regime.

6

Mourad (1990) considered an idealized problem involving 2-D structures in a pure Ekman boundary layer. Restriction to 2-D omits what turns out to be the dominant signature of boundary layer roll vortices: the strong along-roll near-surface enhancement and reduction of the surface wind. He demonstrated that triad wave-wave interactions could allow significant upscale energy transfer from fast-growing modes into the slower growing large scale mode via a spatially resonant third wave, i.e. we have three waves, with amplitudes *A*, *B* and *C*, whose wave numbers satisfy $\alpha = \beta + \gamma$ respectively. In this simplest form, the theory includes nonlinear interaction terms between the three waves only up to the first nonlinear amplitude correction in a system of coupled Landau equations.

Using this model problem as a guide, I developed an equivalent nonlinear theory for 3-D tropical cyclone roll vortices (i.e., including the along-roll wind modification) growing in a realistic hurricane boundary layer flow that is an extension of the theory described in Foster, 2009. The new mean flow includes realistic surface layer fluxes and dynamics and realistic effective and variable eddy viscosity profiles within the hurricane boundary layer. The single-mode hurricane rolls found with this model are an improvement over those presented in Foster (2005)

An example nonlinear resonant triad solution that produces a 10 km wavelength circulation at a twice the radius of maximum winds in a 40 m s$^{-1}$ hurricane is shown in Figure 2. This is a typical flow pattern at quasi-equilibrium in the model. There is a slow lateral inward phase velocity and slow evolution of the multi-scale roll circulation with time as the larger-scale rolls modulate the smaller-scale ones. The basic 2.5 km roll structure embedded in a 1.5 km deep boundary layer remains a dominant feature. However, it is modulated by the 10 km wavelength circulation that, even though it is generated within the boundary layer via the nonlinear wave-wave interaction mechanism, extends over a layer that is about 4 to 5 km deep. Note that the along-wind velocity scale ranges $\pm 8\ to\ 10\ m\ s^{-1}$ and the vertical velocity ranges $\pm\ 3\ to\ 4\ m\ s^{-1}$. Thus, the along-wind velocity perturbations are on the order of $\pm\ 25\%$ of the mean flow
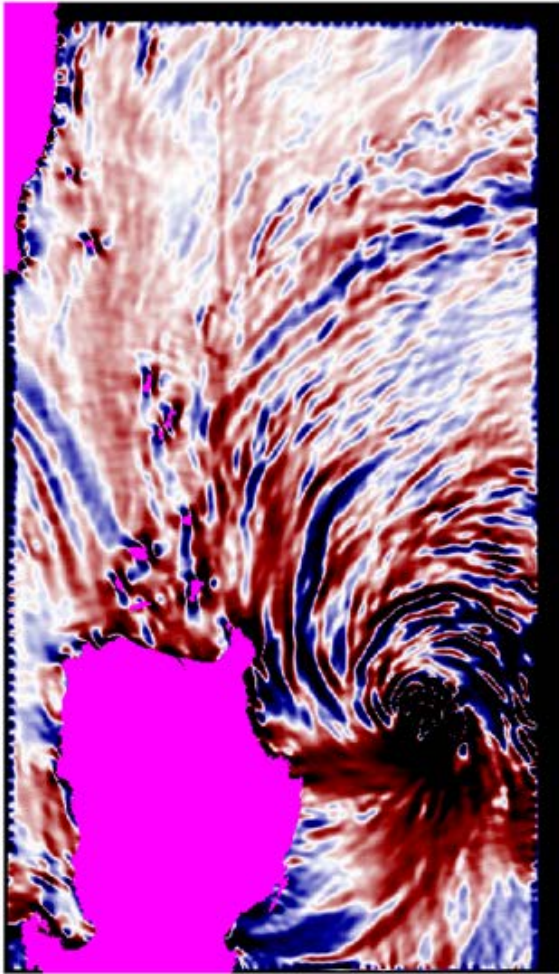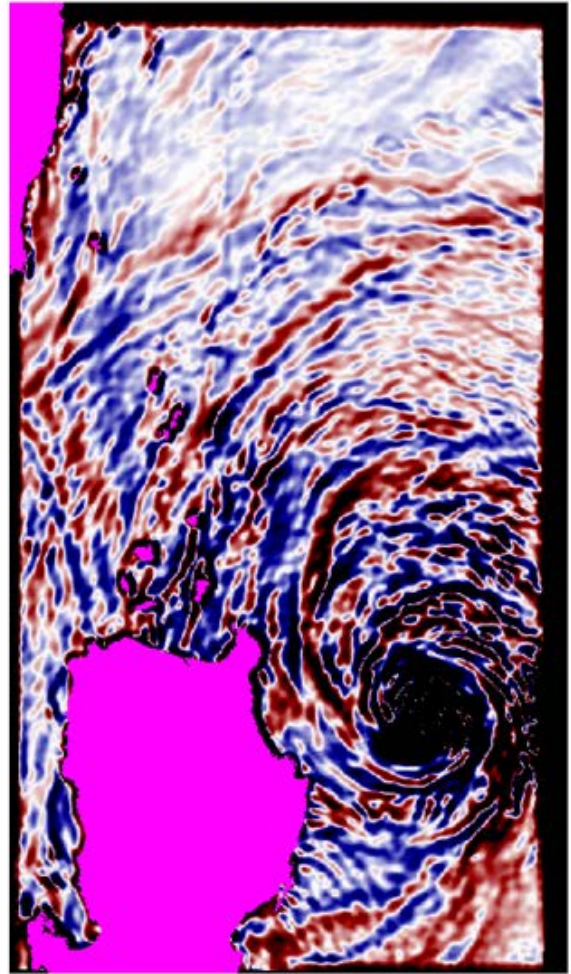
*Figure 4: RadarSAT-2 image of Super-Typhoon Megi just before landfall on Luzon, October 17, 2010. Left: surface wind convergence; Right: kinematic surface wind stress curl.*

There are additional observations that support this mechanism. Gall et al. (1998) presented Doppler radar evidence of ubiquitous 5 km deep, 10 km wavelength roll circulations throughout the landfalls of three hurricanes. They noted that the features they observed had all the characteristics of boundary layer roll vortices, but were of significantly deeper extent and larger wavelength. Hence, we hypothesize that the SAR signatures are the surface manifestation of the Gall et al. (1998) long wavelength, deep rolls. We further hypothesize that they are generated via the nonlinear triad wave-wave mechanism developed as part of this research
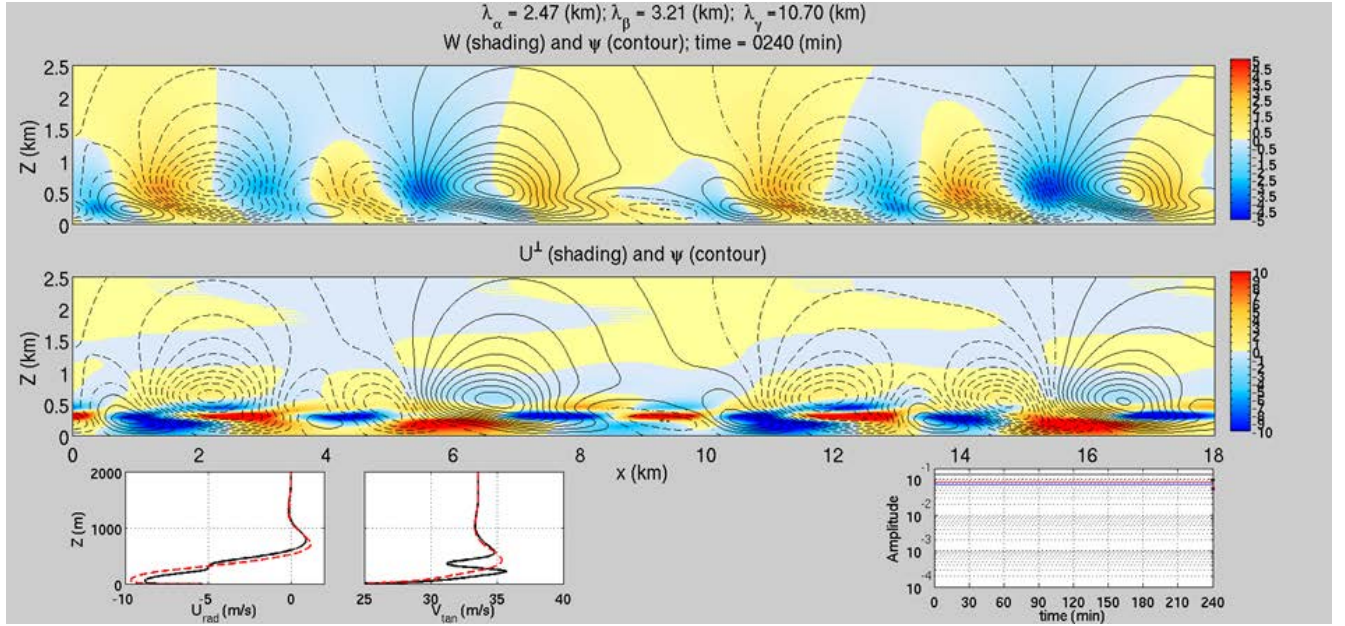
*Figure 5: Typical theoretical solution twice the RMW for nonlinearly interacting resonant triads of boundary layer roll vortices in a 40 m/s hurricane. Top: vertical velocity; Center: Along-roll (mainly along mean wind) velocity. Line contours in both panels is the overturning flow streamfunction. Lower left: red: initial mean flow profile; black: modified mean flow.*

There are aspects of this model that warrant further research. Based on Foster (1997, 2005), I know that truncating the Landau series expansions at the first nonlinear term is a serious limitation. Generally speaking, this truncation tends to over-estimate the nonlinear amplitude of the interacting waves and to exaggerate the modification of the mean flow by the nonlinear solution. Consequently, when calculating single-mode nonlinear solutions, I never include fewer than five high-order Landau coefficients. The exaggerated mean flow modification in these truncated triad solutions can be seen in the lower panels of Figure 2. Calculating the high-order Landau coefficients for a single-wave roll is very difficult (Foster 1997, 2005) and the number of nonlinear interaction terms required to calculate the higher order Landau coefficients increases geometrically. A dedicated research effort will be needed to develop the equations needed to generate the higher-order terms in the multi-wave model.

Another aspect that demands further attention is their possible role in the communication of the surface fluxes of heat, water vapor and momentum and the interior flow above the boundary layer. The theoretical model implies a continuous overturning circulation that extends from the sea surface to well above the PBL top. It will be import to explore whether or not this non-gradient circulation represents an unparameterized contribution to the boundary layer fluxes in numerical models.

Furthermore, the formalism used to generate the nonlinear triad hurricane roll model can be extended to many similar geophysical problems. The methods I used to generate the Matlab solution code are abstracted such that the particular dynamics involved are hidden within the calculation matrices and solution vectors. These are easily modified for different geophysical flows. Hence, it may be relatively simple to convert the existing code into a model for 3-D roll vortices in cold-air outbreaks, which are important factors in high-latitude meteorology. The present model does include temperature and

buoyancy effects. Presently the model assumes co-linear rolls. We could modify the system so that the resonance condition is expanded to include wave vectors instead of just wave numbers. It can also be modified to solve for complex, nonlinear Langmuir cell circulations, which are known to exhibit multi-scale circulations analogous to what we are finding in the hurricane boundary layer. This is another avenue for future research.
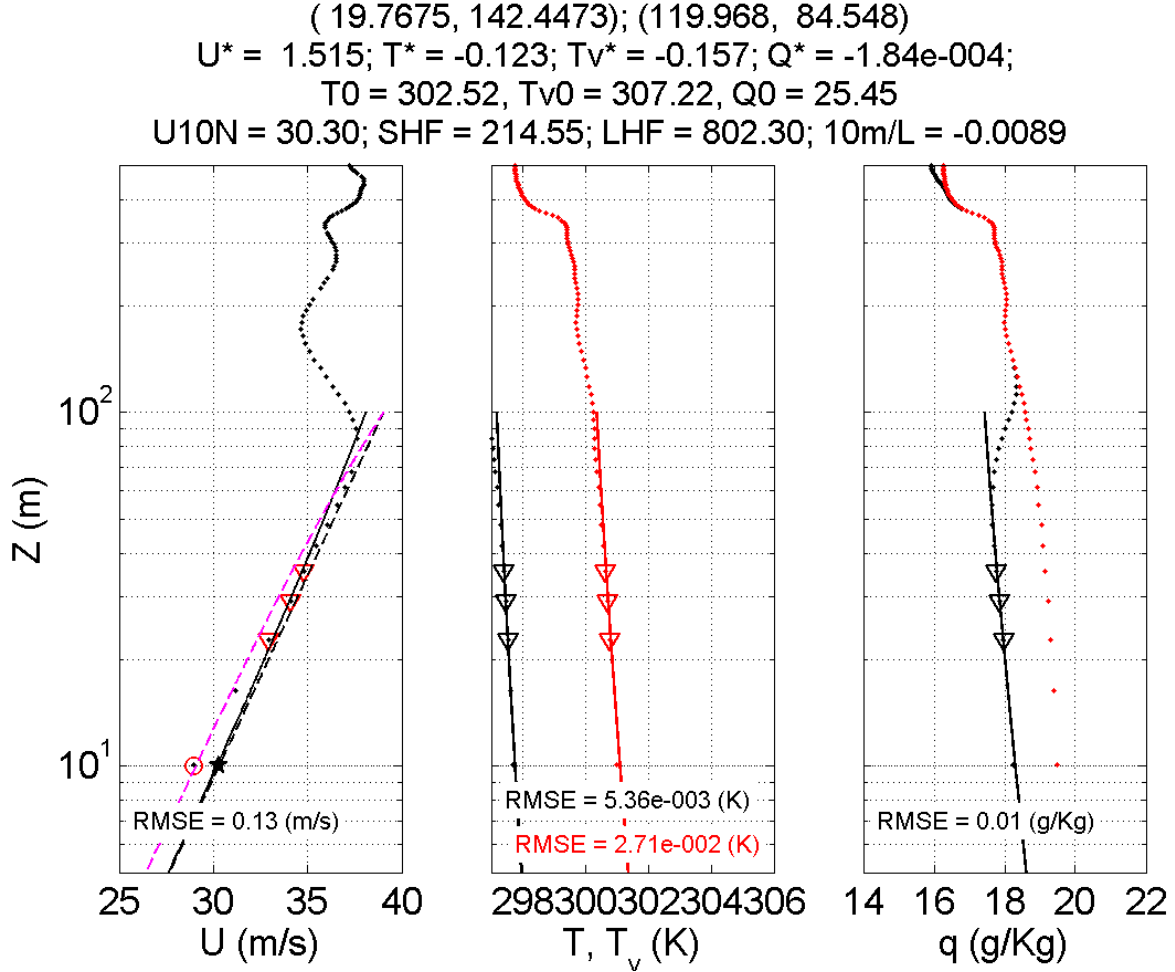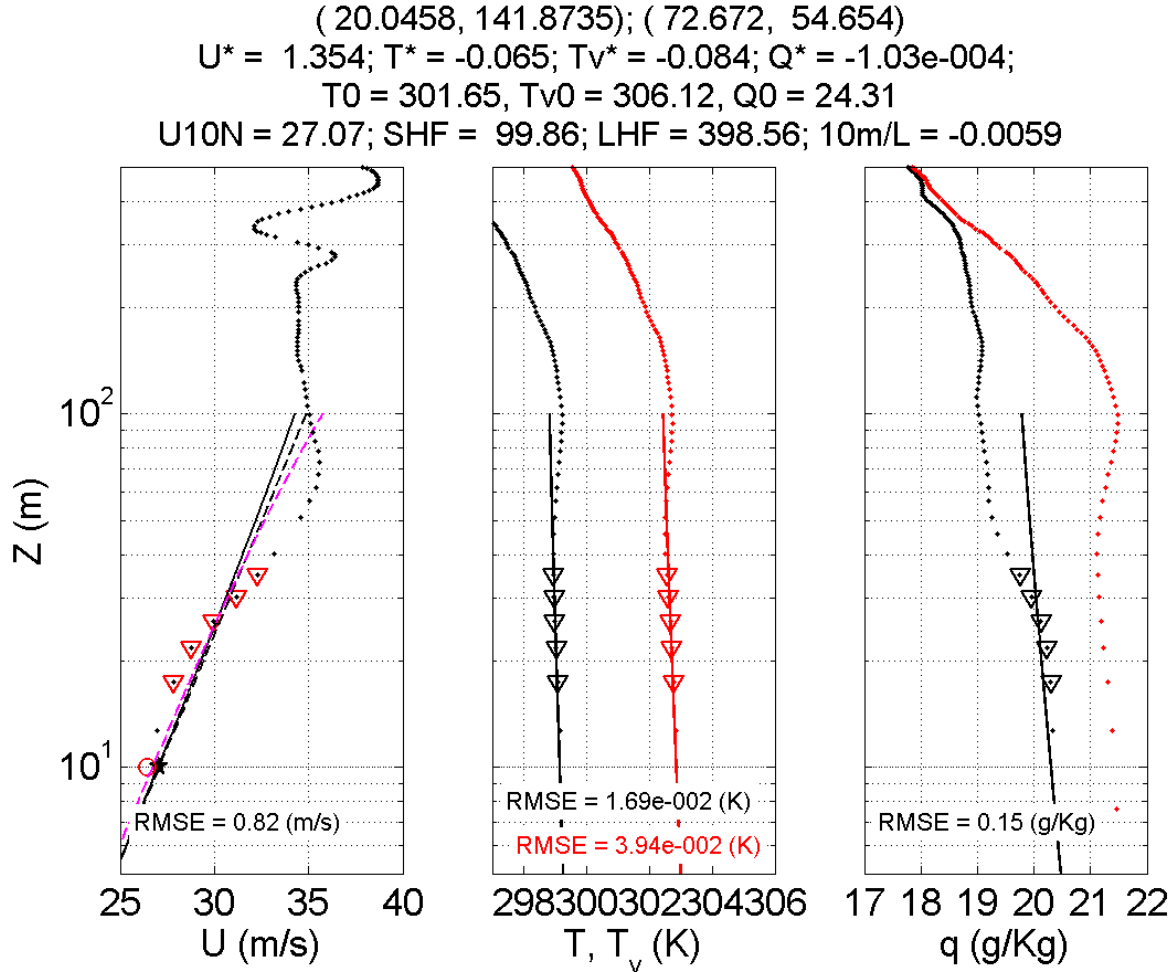


*Figure 6: Drop sonde profile in Typhoon Malakas, 22 Sep, 2010. Sonde data are plotted as dots. The best fit MOS profiles to the wind, temperature and humidity are shown as black lines. In the wind speed plot, the neutral-equivalent MOS profile is the dashed black line. In a log-linear plot, this profile is a straight line. The magenta dashed line is an estimate of the MOS profile from the wind speeds alone, ignoring the temperature and humidity profiles*

## Drop Sonde Analysis

SAR GMFs are designed to estimate the ten-minute average, neutral-equivalent surface wind speed at ten meters above the surface corresponding to the backscatter and viewing geometry. The neutral equivalent wind speed (U10N) is the virtual wind at 10 m that would produce, in a neutrally-stratified boundary layer, the same surface stress as the actual wind in the actual stratification condition. In the high wind region of a tropical cyclone, even though the surface sensible and latent heat fluxes are high, the effective stratification is nearly neutral. Farther from the storm center, the stratification correction becomes more significant.



( 20.0458, 141.8735); ( 72.672, 54.654)
U* = 1.354; T* = -0.065; Tv* = -0.084; Q* = -1.03e-004;
T0 = 301.65, Tv0 = 306.12, Q0 = 24.31
U10N = 27.07; SHF = 99.86; LHF = 398.56; 10m/L = -0.0059

An important part of the ITOP SAR analysis is to make best use of the in situ data colle experiment. We were lucky to have several C-130 flights that were close in time to the SAR overpasses (e.g. Malakas, 22 Sep, 2010). Using the sonde surface pressure for Cal/Val is unambiguous; all that is needed is to make location corrections for the time difference between the splash times and the SAR overpass time. However, using the surface wind information is a subtly difficult problem since sonde surface winds are not ideal for evaluating SAR winds for two reasons: the sonde winds are highly suspect at 10 m and are not necessarily representative of the mean flow.

The calculation of the wind speed from drop sonde profiles is based on very precise knowledge of the sonde's location over very short time intervals. In high shear regions, such as the near-surface part of the hurricane boundary layer, the sampling rate of the GPS is insufficient to calculate wind velocities (Hock and Franklin, 1999). Consequently, simple interpolation of the reported wind speed to 10 m is not a reliable estimate of even the instantaneous surface wind speed even though the sonde profiles frequently extend as low as 6 or 7 m above the surface.

Drop sondes do not measure the *mean* wind, temperature or humidity. They are single snapshot profiles of the highly turbulent boundary layer flow and are not necessarily representative of the mean flow. Near the surface, the standard assumption is that the mean flow profiles follow Monin-Obukhov similarity (MOS), which relates the vertical profiles of wind speed, temperature and humidity to the surface fluxes of momentum, heat and water vapor. Any given snapshot profile might, at first glance, appear to be quite inconsistent with MOS. It is not possible to state confidently whether or such poor agreement is due to MOS being invalid for the particular conditions sampled. Ideally ten or more drop sondes would be deployed simultaneously and the results averaged to produce an approximate mean flow, which could be compared to MOS. If MOS is followed, the surface fluxes (and hence U10N) can be estimated. Currently, this is not possible.
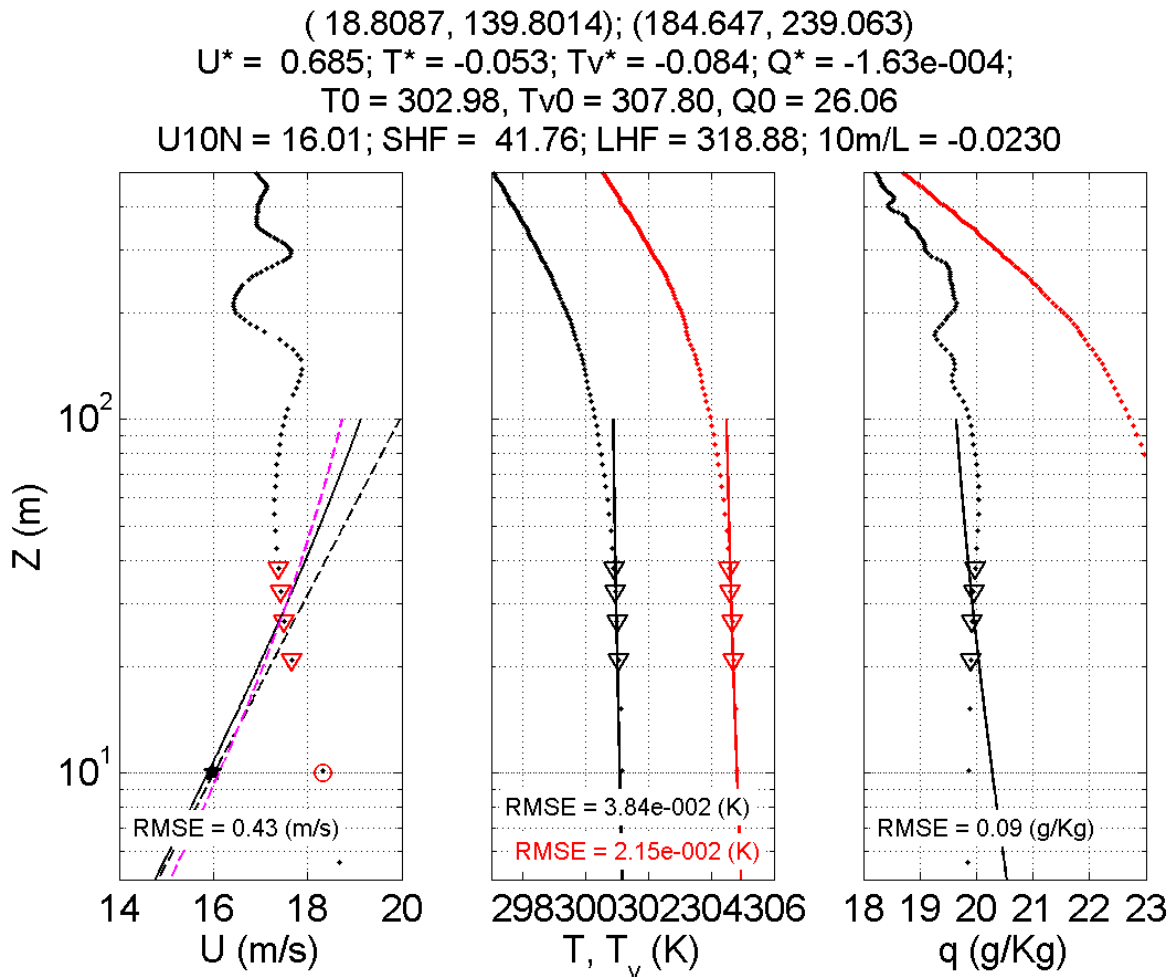


*Figure 8: Challenging sonde profile from Typhoon Malakas, 22 Sep, 2010*

Two methods commonly for estimating U10 use the mean of the lowest 150 m of the sonde profile (U150; Franklin et al., 2003; and Uhlhorn et al. 2007). Franklin et al. (2003) analyzed eyewall profiles and fit a reduction factor that relates U150 to the surface wind as a function of the mean height of the 150 m layer used in the averaging (Z150). Sonde profiles that end as high as 180 m above the surface are used. Uhlhorn et al. (2007) made a linear fit of U10 (interpolated from the sonde profiles) to U150. They found that this was, within measurement error, equivalent to the Franklin method when Z150 ~ 85 m, which corresponds to profiles that extend to approximately 10 m above the surface. Because the parameterization is based on data from all available flights, the inherent averaging used in the curve fit is assumed to address single-realization aspect of sonde profiles.

However, examination of profiles from ITOP calls the U150 surface wind parameterizations into some question. Quite commonly there is clear change in the slope of the wind speed profile well below 150 m that strongly suggests that the upper and lower parts profile contributing to U150 sample parts of the near surface flow that are in different dynamical regimes.

We addressed this problem from a different perspective. We assume that we cannot trust sonde wind speeds at or below about 10 to 15 m above the surface. Furthermore, we assume that the dynamical regime strongly affected by the sea surface extends to approximately 50 or 60 m above the surface. This is a fairly conservative estimate in some cases, but inspection suggested that it does well in separating surface layer data from data that is subjected to more complex boundary layer dynamics. We further made the strong assumption that, even though the particular sonde profile represents a single realization through the turbulent flow, we can treat the measurements at different levels as being independent from each other.

Bulk flux models are a restatement of MOS. We fit the implicit MOS similarity model profiles consistent with the COARE 3.0 bulk flux model (incorporating the CBLAST cap on $C_D^N$) to the wind, temperature and humidity measurements within this layer. Small corrections to the temperature to account for the radial displacement of the sonde during the drop were made. Similarly, we used the SFMR wind speeds to make small adjustments for the radial change in wind speed during the sonde descent. Neither of these corrections made significant differences in the results. When possible we used sea surface temperatures (SSTs) from co-located AXBTs. In other cases we used time- and space-interpolated SSTs from Remote Sensing Systems (RSS). This product combines microwave and IR SSTs and is produced on a 9 km grid. The RSS SSTs were generally with a few tenths of a degree to the AXBT SSTs. The model produces estimates of the MOS scaling variables U*, T* and q* from which estimates of U10N and the surface fluxes can be calculated.

Figure 6 shows an example of a simple to interpret case from typhoon Malakas on September 22, 2010. The estimated U10N, sensible heat flux (SHF) and latent heat flux (LHF) are given in the plot title. In this case, the apparent surface layer extends to about 80 m above the surface. It seems evident that averaging the wind speed over the lowest 150 m of this profile will include winds that are in a different dynamical regime.

Figure 7 presents a very typical sonde profile. In this case the sonde wind speeds appear to vary with height around the best fit MOS profile. Again, averaging the wind speeds up to 150 m would appear to include data from different flow regimes. A notable feature of this case is that the humidity profile also varies around the best fit MOS profile in a way that is correlated with the velocity variations. This was routinely observed in the ITOP drop sondes: the deviations of the wind and humidity observations

from the best fit MOS profiles were correlated with each other. In contrast, in all cases the temperature data agree well with the MOS profile. This indicates that the temperature is mixed by eddies that span a wide range of spatial scales, which leads to excellent agreement with MOS even in snapshot profiles. However, we hypothesize that the humidity and momentum are affected by a selective range of eddies. Likely, the humidity is advected by the same eddies that induce the deviations of the wind speeds from the MOS profile.

A challenging example is shown in Figure 8. In this case, the sonde wind speed seems to increase near the surface, which is incompatible with MOS. Again the temperature profile agrees well with MOS and the deviations of the humidity profile from MOS correlate with the wind speed deviations. The majority of profiles resemble Figure 7. Understanding the profiles that look like Figure 8 is the subject of continuing investigation.

This method for evaluating hurricane sonde data is still under development and will be evaluated through comparisons with coupled model output and available SAR wind data. The different methods of estimating U10 often produce very different estimates, but should be a fairly good test of the methodology, which makes the SAR data valuable for evaluating the drop sondes.

Development of this sonde data analysis model was also supported by the NOPP project "A Unified Air-Sea Interface for Fully Coupled Atmospheric-Wave-Ocean Models for Improving Intensity Prediction of Tropical Cyclones".

**IMPACT/APPLICATIONS**

The strong correlation between the derived SLP and the observations suggests that the Cal/Val optimization strategy has strong potential. Those results should have a significant positive effect on future SAR wind retrievals in TC conditions. This will be pursued in future research.

**PUBLICATIONS**

Papers describing the sea-level pressure retrieval from SAR, the Sea-level pressure-filtered winds and the dynamics of the 10 km wavelength rolls are in preparation.

*Presentations*:

Evidence of and a Theory for 10-Km Wavelength Convergence Lines in Tropical Cyclone Surface Wind Retrievals, R.C. Foster and J Patoux, *International Ocean Vector Winds Science Team Meeting*, Utrecht, Netherlands, 12-14 June, 2012.

Using Surface Pressure Produce Scene-Wide, km-Scale Tropical Cyclone Surface Wind Retrievals from SAR, R.C. Foster, JP Patoux, J Horstmann, C Wackerman, *International Ocean Vector Winds Science Team Meeting*, Utrecht, Netherlands, 12-14 June, 2012.

Organized Multi-Km Surface Stress Convergence Lines in Tropical Cyclone Surface Wind Retrievals, R.C. Foster, *SeaSAR International Workshop*, 18-22 June, Tomoso, Norway.

Using Surface Pressure to Improve Tropical Cyclone Surface Wind Retrievals From SAR, R.C. Foster, JP Patoux, J Horstmann, C Wackerman, *SeaSAR International Workshop,* 18-22 June, Tomoso, Norway.

Evidence for and a Theoretical Model of 10-km Wavelength Tropical Cyclone Boundary Layer Roll Vortices, RC. Foster, *18th Conference on Air-Sea Interaction*, Boston, MA, 8-13 July, 2012.

## REFERENCES

Ellis, Ryan S Businger 2010: Helical circulations in the typhoon boundary layer. *J. of Geophys Res* **115**, D06205, doi:10.1029/2009JD011819

Foster RC 1997: Structure and energetic of optimal Ekman layer perturbations, *J Fluid Mech.*, **333**, 97-123.

Foster, R. C., 2005: Why rolls are prevalent in the hurricane boundary layer. *J. Atmos. Sci.*, **62**:2647–2661.

Foster RC 2009: Boundary-layer similarity under an axi-symmetric, gradient wind vortex. *Bound.-Lay Meteorol*. **131** 321-344.

Franklin, J. L., M. L. Black, and K. Valde, 2003: GPS dropwindsonde wind profiles in hurricanes and their operational implications. *Wea. Forecasting*, **18**, 32–44.

Freilich, MS 2001: Validation of Vector Magnitude Datasets: Effects of Random Component Errors, *J Atmos. Ocean Tech*, **14**, 695-703.

Hock, T. F., and J. L. Franklin, 1999: The NCAR GPS dropwindsonde. *Bull. Amer. Meteor. Soc.*, **80**, 407–420.

Lorsolo S, J L. Schroeder, P Dodge, F Marks Jr. 2008: An Observational Study of Hurricane Boundary Layer Small-Scale Coherent Structures, *Mon Wea Rev*. **136**, 2871-2893

Morrison, I., S. Businger, F. Marks, P. Dodge, and J. A. Businger, 2005: An observational case for the prevalence of roll vortices in the hurricane boundary layer. *J. Atmos. Sci.*, **62**:2662–2673.

Patoux J, RC Foster and RA Brown, 2003: Global pressure fields from scatterometer winds, *J Appl Meteorol.*, **42** 813-826.

Patoux, J Foster RC and RA Brown 2008: An evaluation of scatterometer-derived ocean surface pressure fields, *J Appl. Meteor. Clim*. **47**, 835-853.

Patoux, J, RC Foster and RA Brown, 2011: Cross-validation of scatterometer measurements via sea-level pressure retrieval, submitted to *J Geo Phys. Res*.

Uhlhorn E W, et al., 2007: Hurricane Surface Wind Measurements from an Operational Stepped Frequency Microwave Radiometer, *Mon. Wea Rev*, **135**, 3070-3085.

Zhang, J. A., K. B. Katsaros, P. G. Black, S. Lehner, J. R. French, and W. M. Drennan, 2008: Effects of roll vortices on turbulent fluxes in the hurricane boundary layer. *Bound-Layer Meteor*. **128**, 173-189.